An Improved Method to Detect Riblets on Surfaces in Nanometer Scaling Using SEM

E. Reithmeier and T. Vynnyk

Institute of Measurement and Automatic Control, Nienburgerstr. 17, 30167, Hannover, Germany, eduard.reithmeier@imr.uni-hannover.de

Summary. An improved photometric method for recording a 3D-microtopogrpahy of technical surfaces will be presented. The suggested procedure employs a scanning electron microscope (SEM) as multi-detector system. The improvement in measurement is based on an extended model of the electron detection in order to evaluate the detectors signals in a different way compared to known approaches. The method will be applied on a calibration sphere in order to demonstrate the accuracy of the current approach.

1 Introduction

The micro-topography of technical surfaces (Fig. 1) plays an important role for the functional behaviour of many mechanical parts in machinery. For example a large part of the energy-loss in consequence of turbulent air-flow in aviation occurs due to friction between the hull of the plane and the air flowing around it.

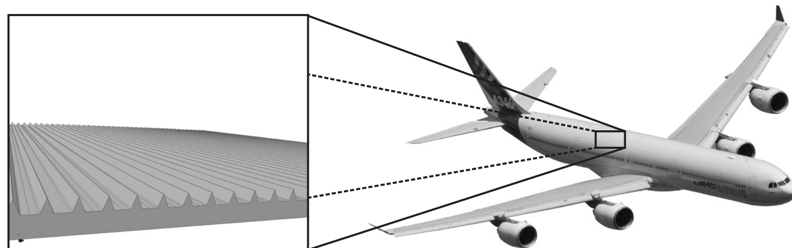

Fig. 1. Riblet structures on airplane

The losses can be reduced considerably by ribbed structures aligned to the flow; so-called riblets. A structure of a trapezoidal shape has been chosen as

base geometry for this research project. The height of these riblet structures is about 20 μm, the approximate period length is about 40 μm, the tip radius lies between 0.1 μm and 0.15 μm and the internal radius between 1-2 μm (see Fig. 2).

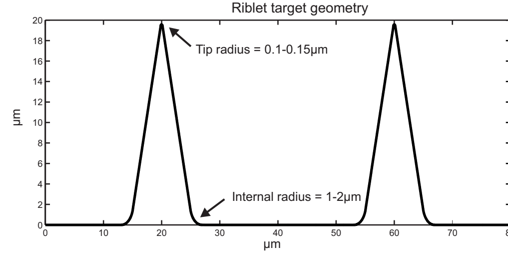

Fig. 2. Trapezoidal base geometry for riblet structures

To ensure the quality of the production process, it is required to measure the manufactured surfaces with a horizontal and vertical resolution up to 20 nm. Due to the large areas of measurement these kind of surfaces needs to be measured fast, sufficiently accurate and, if possible, in non contact mode. Due to the fact that the requested lateral/vertical resolution lies within a range from 10 to 20 nm and that the shape of the surface consists of convex and concave regions, the measurement problem can not be solved using standard measuring tactile or optical methods. For instance, the problem of using a tactile measuring system lies in the insufficient sharpness of the stylus tip. Typically, the tip radius is bigger then 2 μm and the cone angle greater than 60°, see Fig. 3.

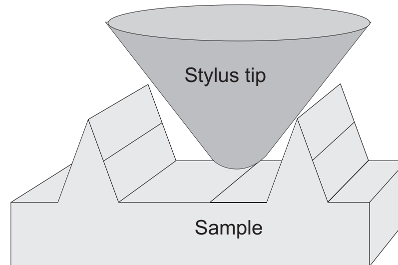

Fig. 3. Problem with the measurement of the concave areas

Due to the high aspect ratio of the riblet structures it turned out that the morphologic filter effects distorts the riblet structures substantially. This distortion is caused by the shape of the stylus tip. A morphologic deconvolution in case of known tip geometry does not lead to an accurate reconstruction

of the profile. Thus tactile measurement technique is only suitable for riblet structures in a very restricted way.

The stylus tip of the most accurate tactile measurement device, namely atomic force microscope, is much smaller, but the maximal measurement range differs between 10 μm and 15 μm. Also, scanning time is too long for the measurement of large areas.

The usage of optical measuring systems is restricted due to the fact that these systems are based on the analysis of the light reflected by the surface of the measured object (See Fig. 4).

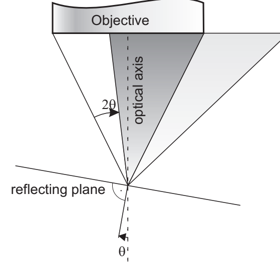

Fig. 4. Problem of direct light reflection at the lateral faces of riblet structures

With increasing tilt angle of the even but rough surface the part of the reflected light cone captured by the objective decreases. Reaching the critical angle the signal to noise ratio finally becomes so bad that the surface cannot be detected anymore. In addition, the horizontal resolution of the best 100x objectives with a numerical aperture NA=0.95 is $d = \frac{\lambda}{2 \cdot NA} \approx \frac{0{,}55 \mu m}{2 \cdot 0{,}95} = 0,29 \mu m$ leads to a value which does not meet the requirements for measurement of the riblet structures.

Employing a scanning electron microscope(SEM) uses an electron beam to take images of the object surface. The electron beam scans the object surface in vacuum. A detector catches the electrons emitted by the surface. In this case the resulting image has much higher optical depth of the field as well as higher lateral resolution. The advantage of the SEM is clearly the higher lateral resolution (approx. 5 nm) in relation to other measuring techniques. The 3D - Surface detection can be realized via stereometric evaluation of the image sequence received at different tilt angles of the specimen. For evaluation all methods require at least 2 images taken at different inclination angles of the specimen. The vertical resolution depends on the lateral resolution and on the tilt angle according to:

$$R_v = \frac{R_h}{\sin(\lambda)} \tag{1}$$

Here R_v is the vertical resolution, R_h is the horizontal resolution, and λ states the tilt angle.

Unfortunately, the inclination angle of the lateral riblet faces is restricted to approximately 10°, due to the limited contrast ration of the SEM images. (Fig. 5: The arrows mark identical points on the topography, which may not be detected in the right image anymore). The typical tilt angle in which

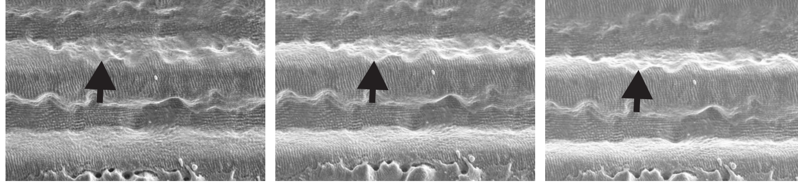

Fig. 5. SEM - images with different tilt angles. Arrows mark identical points in the topography whose similarity is no more recognizable, particularly in the right image

images are still similar, lies within the range of 5 - 7°. By these angles the vertical resolution is approximately 10 times larger than the lateral resolution. To reach a vertical resolution of 0.05 μm, the lateral resolution must lie within the range of 5 nm. Such a high lateral resolution is close to the limit of the SEM - recording technology. Additionally, the final 3d images would have a maximum size of 10 μm x 10 μm, which is insufficient for the measurement of riblet structures due to their period of 40 μm.

2 Solution: Photometric Method

The reconstruction of surfaces from scanning electron microscope (SEM) images is object of extensive research [REI98],[BEI91], [SLO06], but fundamental image processing problems are still unsolved. The approach, described in this paper, uses an alternative model for the image formation. The method is based on the analysis of the secondary electrons registered by the Everhart-Thornley SE detector (Fig. 6).

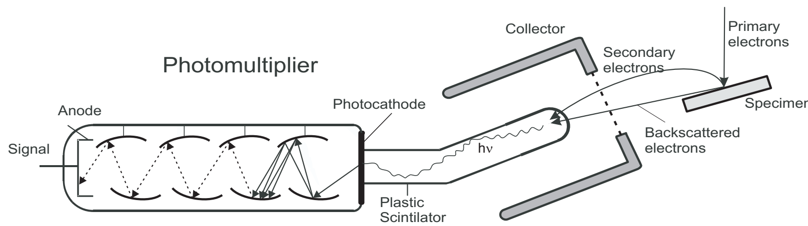

Fig. 6. Everhart-Thornley SE-detector [REI98]

Before the algorithm will be introduced, let us discuss the physical processes occurring during irradiation of the specimen's surface with primary

electrons. The energy of the primary electrons lies in the range of 20-30kV. Electrons, penetrated in the surface, create an electron diffusion region. Depending on the activation type, free electrons of different energy levels are being produced. Inelastic scattering in the area close to the injection hole (0.1-1 nm) yields creation of the low-energy (0-50eV), so called, pure secondary electrons (SE). Deeper areas also produce SE, but their energy is too small to be emitted from the surface, therefore only high-energy back-scattered electrons(BSE) leave the specimen. The typical energy distribution of electrons emitted from the surface of the specimen is shown on Fig. 7. Due to the fact that most part of emitted electrons are SE, only these electrons are essential for 3D analysis of the SEM images. Furthermore, electrons with high energy can be distinguished using SEM images with a negative bias voltage as shown below.

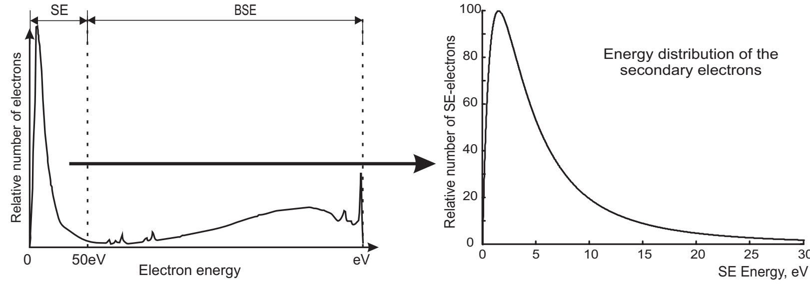

Fig. 7. Energy distribution of the secondary electron's yield(left), low energy distribution(right) [REI98]

The typical energy distribution of SE's is shown on Fig. 7. According to [REI98] the probability density of secondary electrons $f(U_e)$ as function of the electron's energy can be calculated as:

$$f(U_e) = K(U_p)\frac{U_e}{(U_e + W_e)^4}, K(U_p) = \frac{6W_e^2\,(U_p + W_e)^3}{U_p^3 + 3U_p^2 W_e} \tag{2}$$

Here W_e is so called electron's work function, U_p is the energy of the primary electrons and U_e is the energy of the emitted electrons.

According to Lambert's cosine law, the angle distribution of the probability density $g(\varphi)$ may be expressed by:

$$g(\varphi) = \frac{1}{2}\cos(\varphi) \tag{3}$$

φ states the angle between the normal vector of the surface and the emitting direction of the electron.

Using distributions (2) and (3), the distribution of secondary electrons registered by the SE- detector may be expressed by a function of the specimen's tilt angle φ. For this purpose the SE-detector is modelled by an electric

charge, homogeneously distributed on a sphere with a radius r_0. The electron

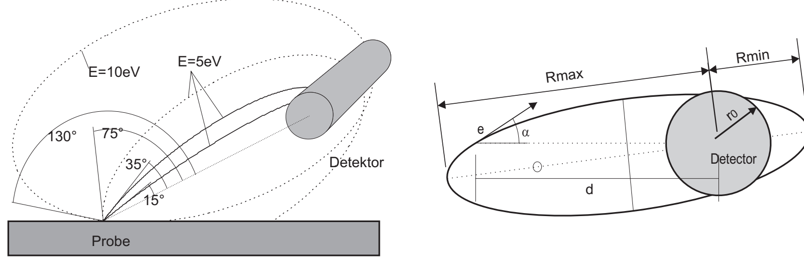

Fig. 8. Possible orbits of electrons

is considered to be registered by SE - detector, if the minimal distance from the centre of the spherical charge is less then r_0. In fact the interaction with the probe also needs to be considered; for simplification however, the influence of the specimen's conducting material is neglected. Due to the nature of electric fields all closed orbits of the electrons have an elliptic shape. According to the laws of energy and momentum conservation, this ellipse is defined by the following parameters:

$$R_{\min} = \frac{-U_d r_0 e + \sqrt{U_d^2 r_0^2 e^2 + 4\left(U_e - U_d r_0 e/d\right) U_e d^2 \sin^2(\alpha)}}{2\left(U_e - U_d r_0 e/d\right)}$$
$$R_{\max} = \frac{-U_d r_0 e - \sqrt{U_d^2 r_0^2 e^2 + 4\left(U_e - U_d r_0 e/d\right) U_e d^2 \sin^2(\alpha)}}{2\left(U_e - U_d r_0 e/d\right)} \quad (4)$$

Obviously, $R_{\min}$ and $R_{\max}$ depend on the angle α, which is the angle between the vector of the initial velocity $v_0 = \sqrt{\frac{2U_e}{m_e}}$ of the electron and the centre of the SE- detector, m_e is the mass of the electron, U_d is the detector bias, U_e is the energy of the emitted electron, r_0 is the radius of the detector, d is the distance to the detector and e is the charge of the electron

If $R_{\max} < r_0$, the electron is considered to have been registered by the SE-detector. Due to the properties of the sine function, for each initial velocity vector v_0 there exists an angle $\alpha_{\max}(v_0, U_d, d)$, for which all electrons with a start angle of [-$\alpha_{\max}(v_0, U_d, d)$...$\alpha_{\max}(v0, U_d, d)$],[$\pi - \alpha_{\max}(v_0, U_d, d)$...$\pi + \alpha_{\max}(v_0, U_d, d)$] will be collected by the SE detector. The amount of registered electrons as function of the angle between surface and detector can be represented as follows:

$$f(\beta) = \int_0^{U\max(=50V)} \frac{U_e}{\left(U_e + W_e\right)^4} \sigma(U_e, \beta) dU_e \quad (5)$$

Here $\sigma(U_e,\beta) := (4\pi)^{-1} \int\limits_{\beta-\alpha_{\max}}^{\beta-\alpha_{\max}} |\cos(\varphi)| \sqrt{\alpha_{\max}^2 - (\varphi-\beta)^2} d\varphi$

The Fig. 9 shows the ration $\sigma(U_e,\beta)$ of the registered to exposed electrons. Low energy electrons are collected by the detector at each tilt angle (left part of the image). With the increasing velocity v_0 of the electrons, $\sigma(U_e,\beta)$ becomes sinusoidal (right part).

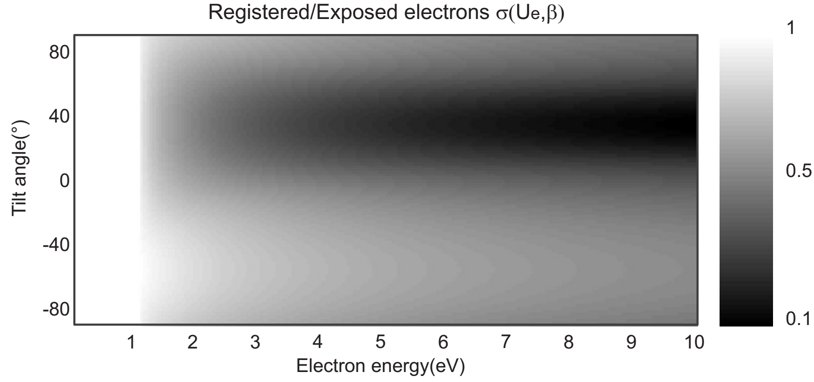

Fig. 9. Ratio of the registered to exposed electrons

As a result $f(\beta)$ and its corresponding Fourier transformation is shown in Fig. 10:

That is $f(\beta)$ may be approximated by

$$f(\beta) = A - B\cos^2(\beta) \tag{6}$$

without loss of the necessary accuracy. This approximation is used for further calculations. Now let us describe the angle β via differential characteristics of the surface with respect to the position of the detector:

$$\mathbf{n}_d = \begin{bmatrix} \cos(\varphi_0) \\ 0 \\ \sin(\varphi_0) \end{bmatrix}, \mathbf{n} = \begin{bmatrix} -\dfrac{\partial Z(x,y)}{\partial x} \\ -\dfrac{\partial Z(x,y)}{\partial y} \\ 1 \end{bmatrix}, \mathbf{n}_z = \begin{bmatrix} 0 \\ 0 \\ 1 \end{bmatrix}$$

Here, n_d is the vector to the SE - detector, n - the normal to the surface and n_z is the vector to SEM electron gun.

The angle between n_d and n vectors can be expressed by:

$$\cos(\beta(x,y)) = \frac{\cos(\varphi_0)\dfrac{\partial Z(x,y)}{\partial x} + \sin(\varphi_0)}{\sqrt{1 + \dfrac{\partial Z(x,y)}{\partial x}^2 + \dfrac{\partial Z(x,y)}{\partial y}^2}} \tag{7}$$

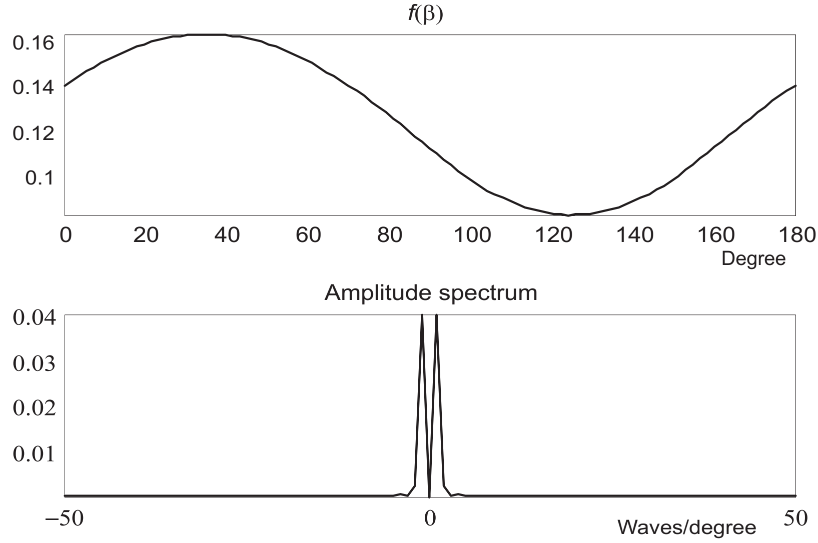

Fig. 10. Angle distribution f_β of the registered electrons and its Fourier transformation

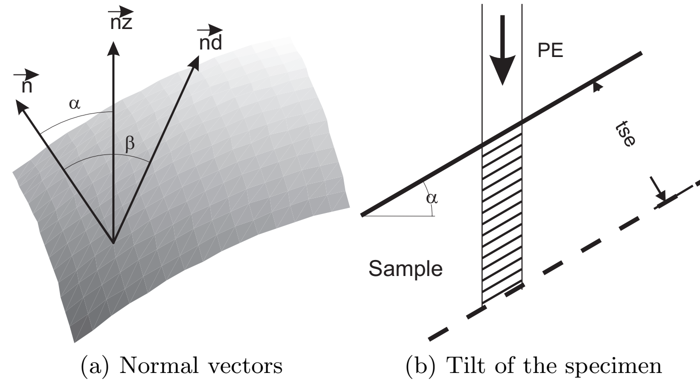

(a) Normal vectors (b) Tilt of the specimen

At this stage the registered portion by the SE-detector will be used for further calculations.

The last step is to define the intensity I_e of emitted SE's as a function of the tilt angle $\alpha(x, y)$:

$$I_e(\alpha(x, y)) = \frac{I_0}{\cos(\alpha(x, y))} = I_0 \sqrt{1 + \frac{\partial Z(x, y)}{\partial x}^2 + \frac{\partial Z(x, y)}{\partial y}^2} \tag{8}$$

Here α is the angle between the tangent plane on the surface mounted in point (x, y) and the direction to the electron gun. Finally, the intensity I_e of electrons, registered by the SE - detector results in

$$I = \sqrt{1 + \frac{\partial Z(x,y)}{\partial x}^2 + \frac{\partial Z(x,y)}{\partial y}^2} \left(C_1 - C_2 \frac{\left(-\cos(\varphi_0)\frac{\partial Z(x,y)}{\partial x} + \sin(\varphi_0) \right)^2}{1 + \frac{\partial Z(x,y)}{\partial x}^2 + \frac{\partial Z(x,y)}{\partial y}^2} \right) \quad (9)$$

This expression will be used for the gradient algorithm, which is presented in the following section. For the surface reconstruction four Everhart-Thornley SE - detectors are used. They are symmetrically positioned in the X-Z and Y-Z planes. The tilt angle of each detector is φ_0 (see Fig. 11).

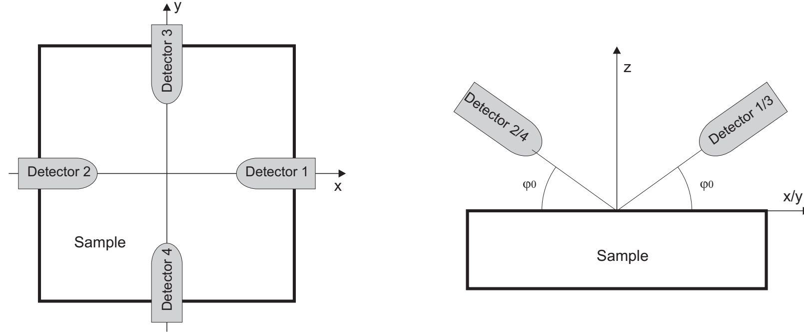

Fig. 11. Measurement setup

2.1 Algorithm

Step 1: Elimination of the BSE electrons. For this purpose each detector will be used twice. Firstly SEM image I^* should be created using a detector bias voltage of -20V. Then the bias voltage must be set to approx. 50V and image I^{**} will be produced. The difference $I = I^{**} - I^*$ serves as basis for further calculations and should be produced for each of the four detectors.
Step 2: Evaluation. According to equation (9) intensities of the collected electrons are estimated as follows:

$$I_{1,2} = \sqrt{1 + \frac{\partial Z(x,y)}{\partial x}^2 + \frac{\partial Z(x,y)}{\partial y}^2} \left(C_1 - C_2 \frac{\left(-\cos(\varphi_0)\frac{\partial Z(x,y)}{\partial x} \pm \sin(\varphi_0) \right)^2}{1 + \frac{\partial Z(x,y)}{\partial x}^2 + \frac{\partial Z(x,y)}{\partial y}^2} \right) \quad (10)$$

$$I_{3,4} = \sqrt{1 + \frac{\partial Z(x,y)}{\partial x}^2 + \frac{\partial Z(x,y)}{\partial y}^2} \left(C_1 - C_2 \frac{\left(-\cos(\varphi_0) \frac{\partial Z(x,y)}{\partial y} \pm \sin(\varphi_0) \right)^2}{1 + \frac{\partial Z(x,y)}{\partial x}^2 + \frac{\partial Z(x,y)}{\partial y}^2} \right) \tag{11}$$

Hence, for each point (x, y) there exist four equations with four unknowns. The Jacobian of the equation system (10)-(11) takes the following view:

$$J = \frac{16 \cdot \cos^4(\varphi_0) \cdot \left(\left(\frac{\partial Z}{\partial x}\right)^2 - \left(\frac{\partial Z}{\partial y}\right)^2 \right) \cdot C_2^2 \cdot \sin^2(\varphi_0)}{1 + \left(\frac{\partial Z}{\partial x}\right)^2 + \left(\frac{\partial Z}{\partial y}\right)^2} \tag{12}$$

According to the inverse function theorem $\frac{\partial Z}{\partial x}$ and $\frac{\partial Z}{\partial y}$ can be uniquely determined, if $J \neq 0$, i.e. $\left|\frac{\partial Z}{\partial x}\right| \neq \left|\frac{\partial Z}{\partial y}\right|$. In that case, combining of I_1, I_2 and I_3, I_4, respectively, yields to:

$$I_1 - I_2 = \frac{-2C_2 \frac{\partial Z(x,y)}{\partial x} \sin(2\varphi_0)}{\sqrt{1 + \frac{\partial Z(x,y)}{\partial x}^2 + \frac{\partial Z(x,y)}{\partial y}^2}} \tag{13}$$

$$I_3 - I_4 = \frac{-2C_2 \frac{\partial Z(x,y)}{\partial y} \sin(2\varphi_0)}{\sqrt{1 + \frac{\partial Z(x,y)}{\partial x}^2 + \frac{\partial Z(x,y)}{\partial y}^2}} \tag{14}$$

Also:

$$I_1 + I_2 - I_3 - I_4 = \frac{2C_2 \left(\frac{\partial Z(x,y)}{\partial y}^2 - \frac{\partial Z(x,y)}{\partial x}^2 \right) \cos^2(\varphi_0)}{\sqrt{1 + \frac{\partial Z(x,y)}{\partial x}^2 + \frac{\partial Z(x,y)}{\partial y}^2}} \tag{15}$$

Combining of (13)-(15) leads to the following linear system of equations:

$$\begin{cases} \dfrac{I_2 + I_1 - (I_3 + I_4)}{I_1 - I_2 + I_3 - I_4} = \dfrac{\frac{\partial Z(x,y)}{\partial y} - \frac{\partial Z(x,y)}{\partial x}}{2\tan(\varphi_0)} \\ \\ \dfrac{I_2 + I_1 - (I_3 + I_4)}{I_3 - I_4 - I_1 + I_2} = \dfrac{\frac{\partial Z(x,y)}{\partial y} + \frac{\partial Z(x,y)}{\partial x}}{2\tan(\varphi_0)} \end{cases} \tag{16}$$

Finally the partial derivatives of the surface are determined by:

$$\begin{cases} \dfrac{\partial Z(x,y)}{\partial x} = 2\tan(\varphi_0)\dfrac{I_2 + I_1 - I_3 - I_4}{(I_3 - I_4)^2 - (I_1 - I_2)^2}(I_1 - I_2) \\ \dfrac{\partial Z(x,y)}{\partial y} = 2\tan(\varphi_0)\dfrac{I_2 + I_1 - I_3 - I_4}{(I_3 - I_4)^2 - (I_1 - I_2)^2}(I_3 - I_4) \end{cases} \quad (17)$$

For the case that $J = 0$, the constant C_2 needs to be predefined. $\frac{\partial Z}{\partial x}$ and $\frac{\partial Z}{\partial y}$ can be determined in this case from (13)-(14)

$$\frac{\partial z}{\partial y}^2 = \frac{(I_3 - I_4)^2}{-(2C_2\sin(2\varphi_0))^2 + (I_3 - I_4)^2 + (I_1 - I_2)^2} \quad (18)$$

$$\frac{\partial z}{\partial x}^2 = \frac{(I_1 - I_2)^2}{-(2C_2\sin(2\varphi_0))^2 + (I_3 - I_4)^2 + (I_1 - I_2)^2} \quad (19)$$

A more realistic description of the problem may be obtained by involving a random function in I_{1-4}. In that sense the signal to noise ratio as well as discretization errors in the measurement of I_{1-4} could be taken into consideration. For $(I_1 - I_2)^2 - (I_3 - I_4)^2 \to 0$, it is recommended to determine constant C_2 via calibration methods and use (18)-(19) for the definition of the partial derivatives .

The main objective, namely to determine the surface $Z(x,y)$ of the measured specimen, can be carried out by numerical integration ([BUL02]) of the partial derivatives $Z_x(x,y)$ and $Z_y(x,y)$. This holds for a certain range of derivatives.

3 Comparing simulation results with a real data

A calibration sphere of a radius r=775 μm was used for the verification of the described approach. The results of the simulation were compared with real data. As measurement device SEM EVO 60 XVP (Fa. Carl Zeiss) was used. This SEM has 1 SE-detector, but includes the feature to rotate around z-axis. This capability was used for taking four images as if there exist four SE - detectors.(Fig. 12):

The measurements detected the spherical structure, with a radius of r=780 μm. The average deviation from the spherical surface lies in the range of $\pm 10\mu$m. The maximal deviation, however, is about 30 μm. Such a big error occurs due to neglecting of the higher frequencies in (6) as well as insufficient precision of I_{1-4} functions (max 256 levels).

4 Conclusion

For simplification it was assumed that the angle distribution of the registered electrons takes the simple form of equation (6). However, this approximation

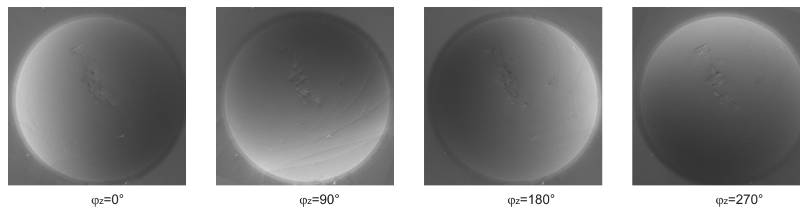

Fig. 12. SEM images from 4 SE-detectors

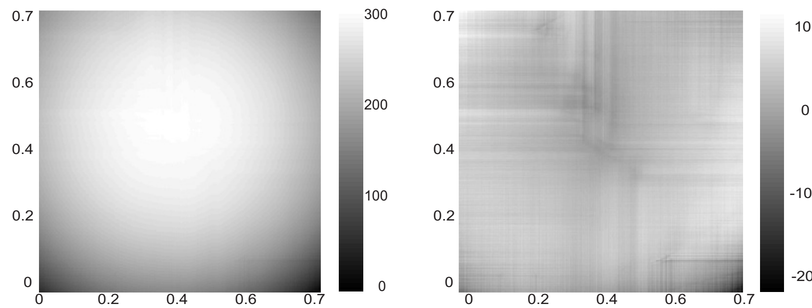

Fig. 13. SEM images from 4 SE-detectors

is not exact and should be expanded. Furthermore, in reality the detector is not spherical, as well as the influence of the specimen's material is not being negligible. As a result the SE intensity distribution should have a more sophisticated form. Nevertheless, these results are very promising and improving the approximations, mentioned above, will certainly lead to even better results.

References

[REI98] Reimer, L.: Scanning Electron Microscopy. Physics of Image Formation and Microanalysis. Springer, Springer, Berlin Heidelberg New York (1998)

[BEI91] Beil, W., Carlsen, I.C.: Surface Reconstruction from Stereoscopy and "Shape from Shading" in SEM Images, Macine Vision and Applications. Vol. 4, 271–285 (1991)

[BUL02] Bulirsch, R., Stoer,J.: Introduction to Numerical Analysis, Springer-Verlag, New York (2002)

[SLO06] Paluszynkski, J., Slowko, W.: Compensation of the shadowing error in three - dimensional imaging with a mutltiple detector scanning electron microscope, Journal of Microscopy. Vol. 224, 93–96 (2006)

[SLO05] Paluszynkski, J., Slowko, W.: Surface reconstruction with the photometric method in SEM, Vacuum. Vol. 78, 533–537 (2005)